Journal of Thermal Science Vol.31, No.2 (2022) 390–406

https://doi.org/10.1007/s11630-022-1575-z **Article ID: 1003-2169(2022)02-0390-17**

Thermodynamic Analysis and Experimental Research of Water-Cooled Small Space Thermoelectric Air-Conditioner

JIANG Fan[1,2,3], MENG Fankai[3], CHEN Lin'gen[1,2*], CHEN Zhaojun[3]

1. Institute of Thermal Science and Power Engineering, Wuhan Institute of Technology, Wuhan 430205, China
2. School of Mechanical & Electrical Engineering, Wuhan Institute of Technology, Wuhan 430205, China
3. College of Power Engineering, Naval University of Engineering, Wuhan 430033, China

Abstract: This paper aims to find a more general analysis method for the refrigeration performance, and to design a high efficiency modular cooling structure of water-cooled plate. A new analysis method, namely current and refrigeration rate density analysis, is proposed. The general refrigeration performance calculation equations are obtained. A finite-time thermodynamic model of the thermoelectric device is established considering Thomson effect. The basic structure of water-cooled thermoelectric air-conditioner is designed and the specific calculation method is given. The influences of input current density, filling factor and heat transfer conditions on refrigeration performance of the thermoelectric air-conditioner are analyzed, which is compared with refrigeration performance of air-cooled thermoelectric air-conditioner. The results show that the maximum refrigeration rate density of the water-cooled thermoelectric air-conditioner is 8.65 kW/m^2, and the maximum coefficient of performance (COP) is 2.27 in the case of the cooling temperature difference ΔT=5 K. Compared with ΔT=5 K, the maximum refrigeration rate density and the maximum COP of ΔT=15 K decreases by 27.98% and 76.65%, respectively. At the filling factor θ=0.43, the refrigeration rate density and COP are 2.57 kW/m^2 and 1.24, respectively. The experimental device of thermoelectric air-conditioner is established to verify the model. The experimental results show that the maximum value of input current and COP is 4 A and 0.95 with the efficient water-cooling method, respectively. The experimental data coincides with the theoretical calculation, which shows the validity of the analysis method and cooling method.

Keywords: thermoelectric air-conditioner, refrigeration rate density, COP, finite-time thermodynamics, non-equilibrium thermodynamics, performance optimization

1. Introduction

People pay more and more attention to environmental problems in the 21st century. Many scientific researchers begin to study new environmentally friendly energy technologies. Thermoelectric devices include the thermoelectric generators, thermoelectric coolers and thermoelectric heat pumps according to different purposes [1–4]. Compared with traditional air-conditioner, thermoelectric air-conditioner has the advantages of small size, no need of harmful refrigerants and safe operation [5, 6]. Thermoelectric air-conditioners can be

Received: Jul 03, 2020 AE: LI Yinshi Corresponding author: CHEN Lin'gen E-mail: lingenchen@hotmail.com 2506715339@qq.com

Nomenclature

A	Area/mm^2	β	Finning coefficients
COP	Coefficient of performance	δ	Thickness/mm
c_p	Specific heat at constant pressure/J·kg^{-1}·K^{-1}	η_f	Fin efficiency
d	Diameter of pipeline/mm	θ	Filling factor
H	Fin height/mm	λ	Thermal conductivity/W·m^{-1}·K^{-1}
h	Heat transfer coefficient/W·m^{-2}·K^{-1}	μ	Thomson coefficient/V·K^{-1}
I	Input current/A	ρ	Electrical resistivity/Ω·m
j	Input current density/A·mm^{-2}	Δ	Difference
L	Length of thermoelectric leg/mm	**Subscripts**	
m	Number of thermoelectric modules	c	Cold junction
N	Number of total thermoelectric elements	cp	Ceramic substrate
Nu	Nusselt number	cv	Convection heat transfer
Pr	Prandtl number	ex	Substrate of junction
p	Cross-section perimeter/m	f	Flow
Q	Heat flow rate/W	fin	Fin
q_h	Heat flow rate density of hot junction/W·m^{-2}	g	Air gap
q_c	Heat flow rate density of cold junction/W·m^{-2}	h	Hot junction
q_1	Heat flow rate density of hot side/W·m^{-2}	one	A thermoelectric module
q_2	Heat flow rate density of cold side/W·m^{-2}	max	Maximum
Re	Reynolds number	mod	Module
R	Total thermal resistance/K·W^{-1}	s	Thermal silicone grease
r	Unit area thermal resistance/mm^2·K·W^{-1}	1	Hot side
T	Absolute temperature/K	2	Cold side
u	Velocity/m·s^{-1}	**Abbreviations**	
v	Kinematic viscosity/m^2·s^{-1}	FTT	Finite-time thermodynamics
Greek symbols		PCM	Phase change material
α	Seebeck coefficient/V·K^{-1}		

applied to air cooling in small space. They have been widely used in biomedicine, electronic device, cryogenic superconductivity [7–10].

In recent years, many researchers have carried out in-depth exploration on single-stage [11–15], two-stage [16–18] and multi-stage thermoelectric coolers [19]. Pietrzyk et al. [11] presented a new characterization factor as a design parameter to simplify the optimization process, and found the impact of contact resistance on the B-factor. Considering many limited conditions, Sun et al. [12] presented a new evaluation approach to evaluate the refrigeration performance, and verified the 3D model by conducting experiments, which proved the rationality of the evaluation approach. Gong et al. [13] studied the refrigeration performance and thermal stress of thermoelectric cooler based on the finite element analysis, which had a great significance to the reliability research on the thermoelectric device. They found the optimal value of thermal stress was 5.4×10^8 Pa approximately. The thermal stress of the basic structure of thermoelectric module was studied by Miao et al. [14]. They found that the deformation was reduced by 6.61% when the optimal number of thermoelectric legs was 20. Wang et al. [15] proposed a new 3D model and found the impact of number ratio of three different structures on refrigeration performance. Different from the traditional two-stage thermoelectric cooler, a new two-stage cascade thermoelectric model was established by Ma and Yu [16]. They explored the impacts of leg length ratio, the temperature of cold side and other factors on comprehensive performance, and found the minimum value of temperature was 257 K. Lin and Yu [17] proposed a trapezoid thermoelectric element structure, which was different from the traditional structure. The results showed that there were optimal shape ratio and length ratio to optimize refrigeration performance. In addition, many researchers have been used some algorithms to optimize the performance. For example, the multi-objective genetic algorithm was used to optimize the thermoelectric device by Meng et al. [18]. They

found the optimal value of COP in the new thermoelectric model was 0.364. Provensi and Barbosa [19] analyzed the refrigeration performance of multi-stage thermoelectric coolers.

Researchers have studied not only the steady-state performance but also the transient performance of thermoelectric coolers [20–23]. A new method to improve the maximum temperature drop of two-stage thermoelectric cooler was presented by Lv et al. [20]. They established a new 3D transient analysis model and analyzed the impact of different cases on supercooling characteristics of devices. Lin et al. [21] studied the impact of some operation parameters on transient characteristics by conducting experiments, and confirmed the conclusion that the two-stage was better than the single-stage. Different from the previous researches, Ruiz-Ortega et al. [22] proposed a novel parameter named the "characteristic cooling length" considering various constraints. They analyzed the refrigeration performance of thermoelectric cooler under current pulse load, and also performed the impact of thermoelectric leg length on the refrigeration performance. In order to design a simple tool to study the transient performance of thermoelectric devices, Fong et al. [23] optimized the design of thermoelectric coolers by adopting a new analytical method, taking into account the given boundary conditions and heat transfer.

Cooling methods of thermoelectric coolers have always been a research hotspot, including air-cooled [24–27], water-cooled [28–36], heat pipe [37, 38], phase change materials (PCM) [39, 40] and so on. Different from the traditional forced convection heat sink, Baldry et al. [24] designed a small-scale natural convection heat sink which could be used in medical devices. They found that the cooling temperature decreased significantly by using this heat sink and the optimal length of the pin was 50 mm. He et al. [25] focused on the relationship between the refrigeration performance parameters of thermoelectric devices and the working voltage of external devices. They found the optimal range of working voltage in heat exchanger on both sides based on experiments, and the COP reached the maximal value when voltages of the thermoelectric module and the fan in hot end were 4 V and 2 V, respectively. Compared with most previous works, Moradikazeroni et al. [26, 27] established new 3D models, which were more complete than 2D models. They studied the heat transfer and structure of heat sink, and got many novel results. The results showed that the type of straight slot could be selected when considering the production costs. As proposed by Moradikazeroni et al. [26], different shapes of heat sink can be used in the heat dissipation of thermoelectric device. Dizaji et al. [28] proposed a new thermoelectric refrigeration system and concentrated on the impact of different working conditions on several refrigeration parameters, such as COP and COP_{max} (the Carnot COP). They carried out experiments and found the maximal value of COP/COP_{max}. Gökçek and Şahin [29] studied a water-cooled thermoelectric cooler based on microchannel heat sinks, focusing on the temperature and COP under different flow rates. The results showed that COP increased by 21.5% and the final temperature decreased by 2.4 K with the increased flow rate. A jet heat sink with low thermal resistance was designed by Karwa et al. [30]. They have experimentally validated their simulation results, and found that the heat sink could improve the refrigeration performance. Lin et al. [31] focused on the effect of three combined devices with different cooling methods on the heat dissipation of LED. They found that the temperature of substrate decreased by 20 K while using the combination of thermoelectric cooler and the water-cooled micro-channel heat sink. Nanofluids can also be used as coolants in the liquid cooling method. Many scholars have studied the nanofluid from the aspects of nano additives [32], volume fraction [33], shape of nanoparticles [34], and convective heat transfer [35]. Ahmed et al. [36] studied the performance of thermoelectric device with different mixing ratios of nanofluids as coolants. They obtained multiple sets of data through experiments, and found the maximum cooling temperature reduced by 4 K. In recent years, the cooling method of heat pipe has been concerned by some researchers and applied in thermoelectric devices. Sun et al. [37] added gravity heat pipe to thermoelectric refrigeration system, established the relevant model and carried out experiments. They found the cooling effect could be significantly improved by using heat pipe. Liu et al. [38] studied the influence of five different cooling methods on the frosting system of thermoelectric cooler. The results showed that COP of the module with the cooling method of the heat pipe is 0.318. Tan and Zhao [39] carried out research on the application of Phase Change Material (PCM) in a new thermoelectric refrigeration system to improve the cooling effect, and found the effect of working conditions and different modules on refrigeration rate and COP. The results showed that the maximum COP was 0.78. A combination of thermoelectric technology and PCM was used in the battery module by Jiang et al. [40]. They found that the time of reaching the maximum temperature was significantly delayed by using PCM.

Finite-time thermodynamics (FTT) is a powerful tool, which combines the theories of heat transfer, thermodynamics and fluid mechanics [41–45]. Some new discoveries can be found for thermoelectric devices [3, 4] by using the FTT theory. Chen et al. [46] analyzed the refrigeration performance based on the FTT theory earlier, and theoretically analyzed and experimentally verified

the relationship between refrigeration rate, COP and input current. Meng et al. [47] presented a FTT model of the thermoelectric cooler with finned heat exchangers and studied the refrigeration rate and COP. Chen et al. [48] proposed a new general method to analyze the air-cooled thermoelectric cooler, concentrating on the influence of the input current, filling factor and other geometry parameters on the refrigeration performance. They obtained design parameters of the heat sink, and found the optimal height of fin. Lu et al. [49] explored the thermoelectric refrigeration system from the aspect of thermal resistance distribution, and carried out experiments to verify the theoretical model. They found the proportion of the optimal thermal resistance distribution. And the COP of thermoelectric module with thermal resistance matching was 0.37, which was higher than that of other ordinary modules. Many researchers studied thermoelectric devices by new methods. Lundgaard and Sigmund [50] proposed a new type of thermoelectric cooler, and analyzed its optimization based on density-based topology optimization method. The results showed that the refrigeration performance was obviously improved. Sun et al. [51] optimized the two-stage series and parallel thermoelectric cooler by using NSGA-II. They obtained the optimal value of the low-level leg length was 1.448 and 1.882, respectively.

The following characteristics can be found by summarizing the published literature:

(1) The Thomson effect is usually neglected to simplify modeling and processing. However, some researchers focused on the Thomson effect and got some important conclusions. Chen et al. [52] found that when considering the Thomson effect, the refrigeration rate was increased by 6.51%. Ruiz-Ortega et al. [53] found that the refrigeration rate and COP of the device with thermoelectric material $(Bi_{0.5}Sb_{0.5})_2Te_3$ increased 3.21% and 9.43% when considering the Thomson effect. Kaushik et al. [54] and Feng et al. [55] revealed that Thomson effect has obvious influences on the performance of thermoelectric devices. Moreover, most people studied the specific structure and commercial thermoelectric modules. However, the calculation method is not universal and not easy to popularize and apply.

(2) Most of the researches on thermoelectric air-conditioner focused on the current, voltage and flow rate. There are few studies on the performance of water-cooled thermoelectric air-conditioners from the geometry of heat exchanger. Few people studied the influence of the geometry of heat exchanger on the performance of water-cooled thermoelectric air-conditioners.

(3) Although a variety of cooling methods are discussed, there is a lack of comparison between different cooling methods especially between water-cooled and air-cooled.

In view of the above problems, this paper attempts to make improvements from the following aspects:

(1) Chen et al. [48] ignored the Thomson effect, simplifying the numerical model and focusing on the air-cooled thermoelectric cooler. Based on the previous work, a more complete FTT model of water-cooled thermoelectric air-conditioner is established considering Thomson effect. A new widely-suited analysis method, namely current and refrigeration density analysis is adopted. The more general result is obtained, and the theoretical model is verified by experiments.

(2) Compared with the structure of heat exchangers proposed by Gökçek and Şahin [29] and Chen et al. [48], a high efficiency modular cooling structure of water-cooled plate is proposed and designed. The influence of heat exchanger geometry parameters on refrigeration performance is studied, such as the thickness and height of fin and pipe diameter of the water-cooled plate. The detailed calculation method of the water-cooled plate and air-cooled of the rib wall is given.

(3) In the numerical simulation, the refrigeration performance of the thermoelectric air-conditioner with water-cooled at the hot side and air-cooled at the cold side is studied, and compared with air-cooled on both sides under the same working conditions. The refrigeration performance of the new high efficiency cooling method with water-cooled plate is verified and analyzed by conducting experiments.

The Thomson effect is neglected by many scholars. And most of calculation methods of water-cooled thermoelectric air-conditioner are not universal. Therefore, the purpose of this paper is to present a more general model, design structure and calculation method of water-cooled thermoelectric air-conditioner so that the results are closer to the actual work condition. In addition, the influences of input current density and geometric parameters of heat exchanger on the refrigeration performance are studied. An experimental device of thermoelectric air-conditioner is established to verify the model. The results are expected to provide guidance for the design and operation of water-cooled thermoelectric air-conditioner.

2. Description of Problem

In order to simplify the model, many scholars neglected the Thomson effect when building the numerical model. In addition, most of the studies have used specific thermoelectric modules, such as TEC-12705, TEC-12706, etc. But the calculation methods in those studies are not universal enough.

Moreover, most of the researches on water-cooling have only specific experimental data and no detailed calculation method.

In this paper, the numerical model is built by considering Thomson effect, so the result is closer to the actual situation. A new widely-suited analysis method, namely current and refrigeration density analysis is adopted, which can be used to get more general results. A high efficiency modular cooling structure of water-cooled plate is proposed and designed.

Fig. 1 gives the control volume of the system. Fig. 2(a) shows the structure of a water-cooled thermoelectric air-conditioner. Fig. 2(b) presents the three-dimensional structure of the thermoelectric air-conditioner. The geometry of the heat exchanger affects the refrigeration rate density and COP of the device. In this paper, the effects of the pipe diameter in the water-cooled plate, the thickness and the height of the fin on the refrigeration performance are studied.

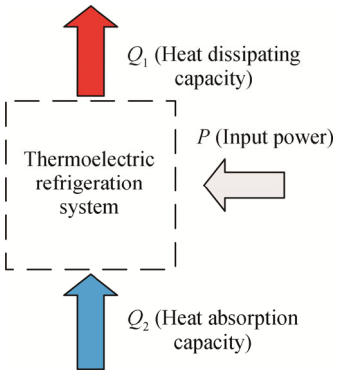

Fig. 1 The thermodynamic system

3. Device Structure and New Analysis Method

In Fig. 2, the device is mainly divided into two parts: thermoelectric modules and two heat exchangers. The hot junction of the device is a water-cooled plate, and the cold junction is an air-cooled heat sink with a fan.

The secondary side is assumed to be adiabatic in this study. According to the theory of non-equilibrium thermodynamics, the refrigeration performance of thermoelectric air-conditioner is related to the number of thermoelectric modules. In order to make the results universal and reflect the refrigeration performance of the same module area, the refrigeration rate density analysis method is used. Therefore, the heat flux densities at two junctions of the device are

$$q_h = \left[\frac{1}{2}\alpha j T_h - \frac{1}{L}\lambda\left(T_h - T_c\right) + \frac{1}{2}L\rho j^2 - \frac{1}{2}\mu j\left(T_h - T_c\right)\right]\theta \tag{1}$$

$$q_c = \left[\frac{1}{2}\alpha j T_h - \frac{1}{L}\lambda\left(T_h - T_c\right) - \frac{1}{2}L\rho j^2 + \frac{1}{2}\mu j\left(T_h - T_c\right)\right]\theta \tag{2}$$

where α, λ, ρ and μ are the Seebeck coefficient, thermal conductivity, conductivity and Thomson coefficient, respectively. The Thomson coefficient is $\mu=T(\mathrm{d}\alpha/\mathrm{d}T)$. T_h and T_c are temperatures of two junctions. L and θ are the length of the thermoelectric element and filling factor, respectively. j is the input current density, and it is $j=I/A$ (I and A are input current and cross-section area of thermoelectric element respectively).

The filling factor θ is

$$\theta = 2AN/A_{mod} \tag{3}$$

where N is the number of total thermoelectric elements; A_{mod} is the total area of modules; A is the cross-section area of thermoelectric element.

The filling factor is the ratio of cross-section area of thermoelectric elements to thermoelectric module area. As shown in the Eqs. (1) and (2), the heat flux densities at two junctions are proportional to the filling factor. At a fixed input current density, the larger the filling factor is, the greater the heat flux density is. In addition, the filling factor can enhance with the increases of the cross-section area or the number of thermoelectric elements. Then the heat flux density will increase. Commercial thermoelectric modules mostly adjust their refrigeration performance by changing the cross-section area of elements.

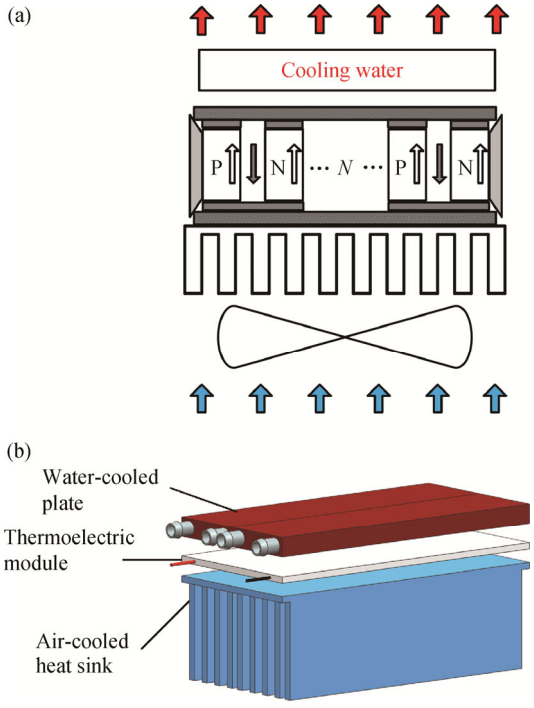

Fig. 2 Structure of the thermoelectric air-conditioner

The heat flux density at cold junction also can be called refrigeration rate density. The refrigeration rate density q_c can also be calculated by:

$$q_c = \frac{Q_c}{A_{mod}} \tag{4}$$

$$A_{mod} = A_{one} \cdot m \tag{5}$$

where Q_c is the refrigeration rate; A_{mod} is the total area of modules; A_{one} is the area of one module; m is the total number of modules in the thermoelectric device.

Besides, the maximum refrigeration rate density $q_{c,max}$ and the input current density $j_{q,max}$ are

$$q_{c,max} = \frac{\theta}{L}\left[\frac{(\mu\Delta T)^2 + 2\mu\alpha T_c\Delta T + (\alpha T_c)^2}{8\rho} - \lambda\Delta T\right] \tag{6}$$

$$j_{q,max} = \frac{\alpha T_c + \mu\Delta T}{2\rho L} \tag{7}$$

where ΔT is the refrigeration temperature difference.

When the Thomson effect is ignored (μ=0), Eqs. (6) and (7) are simplified as follows

$$q_{c,max} = \frac{\theta}{L}\left[\frac{(\alpha T_c)^2}{8\rho} - \lambda\Delta T\right] \tag{8}$$

$$j_{q,max} = \frac{\alpha T_c}{2\rho L} \tag{9}$$

It can be seen from Eqs. (6)–(9) that $q_{c,max}$ with the Thomson effect is higher than that of without the Thomson effect. In addition, the shorter the length of thermoelectric leg, the higher the temperature of cold junction, the larger the optimal input current density is. The larger the filling factor, the smaller the length of thermoelectric element and the smaller the temperature difference, the larger the refrigeration rate density is. On the contrary, with increased filling factor, the area of thermoelectric element in the thermoelectric module increases. And the air gap decreases, the convection and the heat absorption in the module decreases.

Heat transfer in thermoelectric devices can be simplified to one-dimensional heat transfer. The thermal resistance of heat exchanger is affected by the device size, so it can reflect the external heat transfer performance. In order to simplify the calculation, the unit area thermal resistance r can be used to replace the total thermal resistance R_{ex}, and that is r=$R_{ex}A_{mod}$. The boundary conditions are the temperature T_1 of heat reservoir and the temperature T_2 of cold reservoir.

The heat flux densities of hot and cold sides are given by

$$q_1 = \frac{T_h - T_1}{r_1} \tag{10}$$

$$q_2 = \frac{T_c - T_2}{r_2} \tag{11}$$

where T_1 and T_2 are temperatures of two reservoirs; r_1 and r_2 are the unit area thermal resistances of two sides, respectively.

According to the energy balance of the system, there are

$$q_1 = q_h \tag{12}$$

$$q_2 = q_c \tag{13}$$

$$\mathrm{COP} = \frac{q_2}{q_1 - q_2} \tag{14}$$

Because q_h and q_c are used to describe the heat flux density of two junctions of the thermoelectric air-conditioner in Eqs. (1) and (2), therefore, they are regardless of the modules number and the thermocouples number. q_h and q_c can be calculated by several different physical parameters (λ, ρ, α), and geometric parameters (A, L) of various sizes of thermoelectric air-conditioners. Eqs. (10) and (11) are suitable for various heat transfer methods such as air cooling and water cooling. Ignoring the thermal heat transfer of the secondary side and substituting Eqs. (1), (2), (10) and (11) into Eqs. (12) and (13), the performance of the thermoelectric air-conditioner can be calculated for given conditions of heat reservoir and heat transfer.

4. Thermal Resistance Network Analysis

Fluid dynamics or heat transfer can be reflected by the change of thermal resistances, so the thermal resistances are analyzed. The thermal resistance network diagram is given in Fig. 3. Fig. 4 shows the structures of water-cooled plate and heat sink.

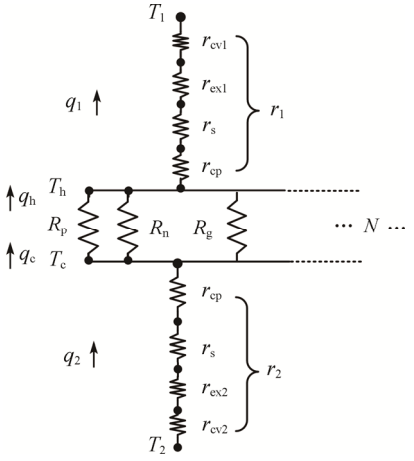

Fig. 3 Thermal resistance network

There is a certain temperature drop between heat sink and modules. Thus, the contact thermal resistance of thermal silicone grease is

$$r_s = \delta_s/\lambda_s \tag{15}$$

The thermal resistances of two junction substrates and module ceramic substrate are, respectively:

$$r_{ex1} = \delta_{ex1} / \lambda_{ex1} \quad (16)$$

$$r_{ex2} = \delta_{ex2} / \lambda_{ex2} \quad (17)$$

$$r_{cp} = \delta_{cp} / \lambda_{cp} \quad (18)$$

where δ_s, δ_{ex} and δ_{cp} are the thickness of thermal silicone grease, substrate of junction, and ceramic substrate, respectively. λ_s, λ_{ex} and λ_{cp} are the thermal conductivity of thermal silicone grease, substrate of junction, and ceramic substrate, respectively.

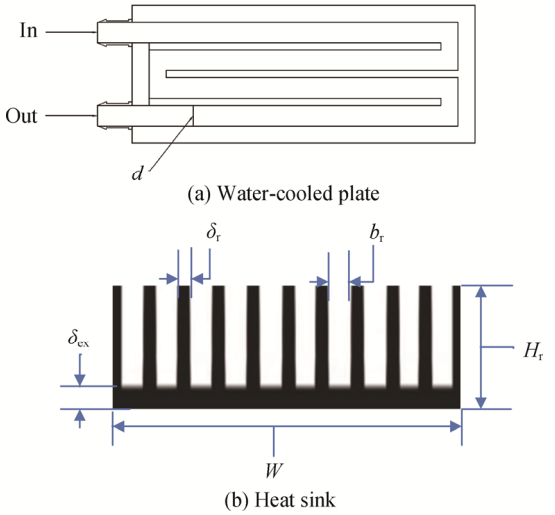

Fig. 4 Structures of water-cooled plate and heat sink

The cooling water is forced to flow in water-cooled plate and absorbs heat, which makes the temperature increase. The heat transfer resistance is [56]

$$r_{cv1} = 1/h_1 \quad (19)$$

The heat transfer coefficient h_1 can be calculated by

$$h_1 = \frac{\lambda_f}{d} Nu_f \quad (20)$$

where d is the diameter of pipe; λ_f is the thermal conductivity; Nu is the Nusselt number.

Considering the flow state of water in the pipe, the turbulence correlation (the Dittus-Boelter equation) of forced convection heat transfer in the tube can be selected [27]. The Nusselt number Nu is

$$Nu_f = 0.023 Re_f^{0.8} Pr_f^{0.4} \quad (21)$$

where the Reynolds number is $10^4 \leq Re_f \leq 1.2\times10^5$; the Prandtl number is $0.7 \leq Pr_f \leq 120$.

The Reynolds number Re is

$$Re_f = \frac{ud}{v_f} \quad (22)$$

where u is the water flow velocity; v_f is the kinematic viscosity.

Air at the cold junction is forced air-cooled of the rib wall. The most common cross-section straight heat sink with equal section is used in this calculation. Therefore, the heat transfer resistance is [57, 58]

$$r_{cv2} = 1/(\beta h_2 \eta_f) \quad (23)$$

where η_f is the fin efficiency of heat sink; β is the rib effect coefficient of heat sink.

The fin efficiency η_f is [57, 58]

$$\eta_f = \tanh(mH)/mH \quad (24)$$

$$mH = \sqrt{(h_{fin} p_{fin})/(\lambda_{fin} A_{fin})} \cdot H_{fin} \quad (25)$$

where h_{fin}, A_{fin}, p_{fin}, λ_{fin} and H_{fin} are heat transfer coefficient, area, cross-section perimeter, thermal conductivity and height of the fin, respectively.

Air gap thermal resistance is

$$r_g = L / \lambda_{air} \quad (26)$$

where L is the length of the thermoelectric element; λ_{air} is the air thermal conductivity.

5. Parameter Influence Analyses

The low temperature thermoelectric material bismuth telluride (Bi_2Te_3) is used to calculate the physical property parameters at the average temperature of the cooling water and the air. Considering variable physical properties of thermoelectric material Bi_2Te_3 [59, 60], the physical property parameters are given as follows

$$\alpha = (22\,224.0 + 930.6T - 0.9905T^2)10^{-9} \text{ V/K} \quad (27)$$

$$\rho = (5112.0 + 163.4T + 0.6279T^2)10^{-10} \ \Omega\cdot\text{m} \quad (28)$$

$$\lambda = (62\,605.0 - 277.7T + 0.4131T^2)10^{-4} \text{ W/(m·K)} \quad (29)$$

$$\mu = (930.6T - 1.981T^2)10^{-9} \text{ V/K} \quad (30)$$

The merit value (ZT) of Bi_2Te_3 is 0.80 at the temperature 348 K. The parameters of air can be obtained by the calculation formulas of air density and specific heat capacity. The relevant parameters in the calculations are set as: α=4.58×10^{-4} V/K, λ=1.649×10^{-4} W/(m·K), ρ=5.424×10^{-10} Ω·m, μ=1.026×10^{-4} V/K, L=2 mm, A=2.07 mm^2, λ_{cp}=35.3 W/(m·K), δ_{cp}=1 mm, δ_{ex}=5 mm, c_{p1}=4.2 kJ/(kg·K), c_{p2}=1.005 kJ/(kg·K). In the numerical simulation, the value range of input current density is 0.1 A/mm^2 to 8 A/mm^2, the value range of air flow velocity is 1 m/s to 10 m/s, and the value range of cooling water flow velocity is 1 m/s to 5 m/s.

5.1 Design parameter analysis

5.1.1 The influence of current density

Figs. 5 and 6 show the relationship between the cold and hot junction temperatures and input current density under different cooling methods. From Fig. 5, the hot junction temperature of thermoelectric module gradually raises with increased input current density. The increase of hot junction temperature in the air-cooled thermoelectric air-conditioner is more significant than the water-cooled. That is, because the heat capacity of water is much larger than that of air. When the input current density increases from 0.1 A/mm^2 to 3.0 A/mm^2, the hot

junction temperature is lower than 303 K, which is significantly lower than the rated maximum temperature of most thermoelectric modules. From Fig. 6, the cold junction temperature of the water-cooled thermoelectric air-conditioner with increased input current density is lower than that of the air-cooled, which indicates that the water-cooled air-conditioner has a larger refrigeration rate density and COP. When ΔT increases from 5 K to 15 K, the cold junction temperature declines for given input current density. For instance, when input current density j is 2.5 A/mm^2, ΔT is 5 K, 10 K and 15 K, and the cold junction temperature of water-cooled is 281.39 K, 278.71 K and 276.04 K, respectively. In Table 1, the hot junction temperature of water-cooled is 300.39 K, which is 16.79 K lower than that of air-cooled in the case of the cooling temperature difference ΔT=5 K and input current density j=2.5 A/mm^2. And the cold junction temperature of water-cooled is 7.07 K lower than that of air-cooled.

Figs. 7 and 8 show the relationship between the refrigeration performance, cooling temperature difference ΔT and input current density under different cooling methods. It should be noted from the figures that there is an optimal input current density, so that the refrigeration performance parameters of the device can reach the maximum value. As the input current density is continuously increased, both the refrigeration performance parameters increase first, and then decrease after reaching the maximum value. As indicated in Figs. 7 and 8, when ΔT increases from 5 K to 15 K, the refrigeration rate density and the COP decrease.

When the secondary side is assumed to be adiabatic, changing the input current density can influence the heat

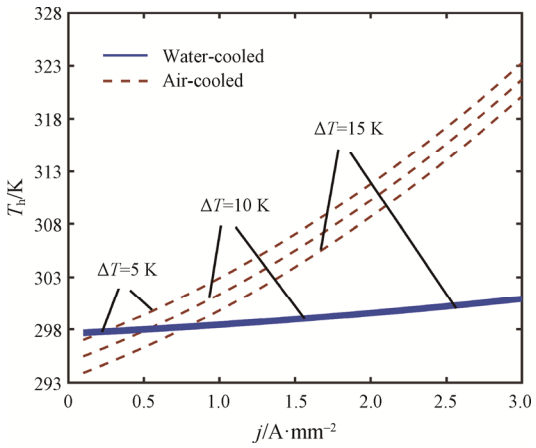

Fig. 5 The hot junction temperature versus input current density under different cooling methods

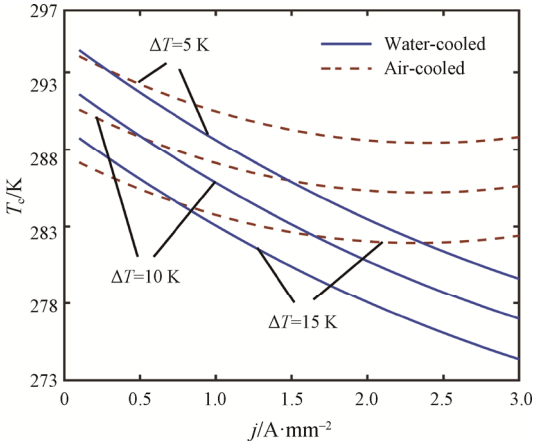

Fig. 6 The cold junction temperature versus input current density under different cooling methods

Table 1 The cold and hot junction temperatures of two thermoelectric air-conditioners at input current density j=2.5 A/mm^2

	The water-cooled air-conditioner			The air-cooled air-conditioner		
ΔT/K	5	10	15	5	10	15
T_h/K	300.39	300.20	300.00	317.18	315.63	314.07
T_c/K	281.39	278.71	276.04	288.46	285.21	281.97

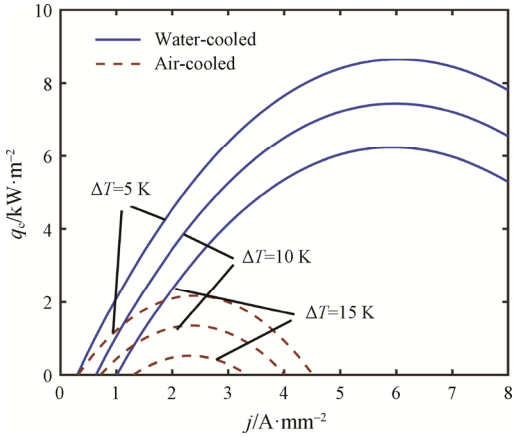

Fig. 7 Refrigeration rate density versus input current density under different cooling methods

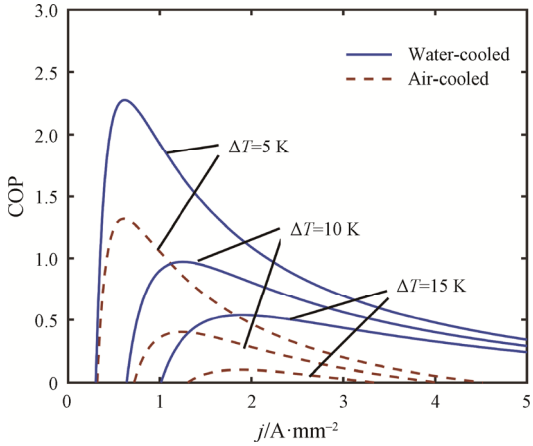

Fig. 8 The COP versus input current density under different cooling methods

flux density of the Peltier, Thomson and Joule effects. The Peltier effect and Thomson effect are beneficial to improve refrigeration performance, while the Joule effect plays a negative role. As the increase of input current density, the cooling effect is obvious because of the Peltier effect and Thomson effect, but the Joule heat raises gradually. Therefore, after the optimal input current density, the Joule effect dominates and the refrigeration performance decreases by continually increasing input current density.

Table 2 lists the optimal performance of two different thermoelectric air-conditioners. In the water-cooled thermoelectric air-conditioner, when the cooling temperature difference ΔT decreases from 15 K to 5 K, the maximum refrigeration rate density increases from 6.23 kW/m^2 to 8.65 kW/m^2, and the COP increases from 0.53 to 2.23. When ΔT decreases from 15 K to 10 K, the maximum refrigeration rate density increases from 6.23 kW/m^2 to 7.44 kW/m^2, and the COP increases from 0.53 to 0.97. The reason is that the increase of cooling temperature difference affects the heat absorption of the cold junction. Therefore, it is necessary to reduce the cooling temperature difference in practice. At ΔT=5 K, the input current density of the maximum refrigeration rate density of the water-cooled thermoelectric air conditioner is 6.04 A/mm^2, and the input current density corresponding to the maximum COP is 0.62 A/mm^2. Considering the cooling effect, economy and safety of the water-cooled thermoelectric air-conditioner, the best input current density range should be 0.62 A/mm^2 to 6.04 A/mm^2.

One can observe from Table 2 that at cooling temperature difference ΔT = 5 K, the maximum refrigeration rate density in the water-cooled thermoelectric air-conditioner is 6.49 kW/m^2 higher than that of in the air-cooled thermoelectric air-conditioner, and the maximum COP is increased by 73.82%. At ΔT=10 K, the maximum refrigeration rate density in the water-cooled thermoelectric air-conditioner is 6.11 kW/m^2 higher than that of in the air-cooled, and the maximum COP is increased by 136.59%. On the other hand, the input current density of the maximum refrigeration rate density is 6.04 A/mm^2 in the water-cooled thermoelectric air-conditioner at ΔT=5 K. And the input current density is 2.39 A/mm^2 in the air-cooled thermoelectric air-conditioner. That is, under the same cooling temperature difference, the input current density of the maximum refrigeration rate density of water-cooled thermoelectric air-conditioner is much larger than that of air-cooled, which is caused by the large difference between the heat capacity of air and water. However, the input current density corresponding to the maximum COP of the water-cooled is slightly larger than that of air-cooled.

Table 2 Optimal performance of two different thermoelectric air-conditioners

	The water-cooled air-conditioner			The air-cooled air-conditioner		
ΔT/K	5	10	15	5	10	15
$q_{c,max}$/kW·m^{-2}	8.65	7.44	6.23	2.16	1.33	0.50
j_q/A·mm^{-2}	6.04	5.98	5.92	2.39	2.37	2.32
COP$_{max}$	2.27	0.97	0.53	1.31	0.41	0.10
j_{COP}/A·mm^{-2}	0.62	1.25	1.90	0.61	1.24	1.85

The heat transfer resistance of water-cooled is less than that of air-cooled, so the heat dissipation performance of water-cooled is better. With increased input current density, the heat accumulated at hot junction cannot be dissipated, and transfers to the cold junction forming heat leakage, so the refrigeration rate density decreases. The heat dissipation of water-cooled can maintain the lower temperature of hot junction. Therefore, whether the optimal value or the maximum value, the input current density of the water-cooled thermoelectric air-conditioner is higher than that of air-cooled.

5.1.2 The influence of module filling factor

The relationship between the filling factor and the refrigeration performance of the device is shown in Fig. 9. Referring to this figure, the refrigeration rate density will enhance with increased the filling factor θ from 0.2 to 0.8, but the COP will decrease. That is because increasing the cross-section area of thermoelectric unit by raising the filling factor leads to the increase of heat flux density, which can also influence the refrigeration rate density. Therefore, when selecting thermoelectric modules, it is necessary to select an appropriate filling factor. The filling factor θ of thermoelectric module made in China is usually in the range of 0.2 and 0.5. At the filling factor θ=0.43, the refrigeration rate density and COP are 2.57 kW/m^2 and 1.24, respectively.

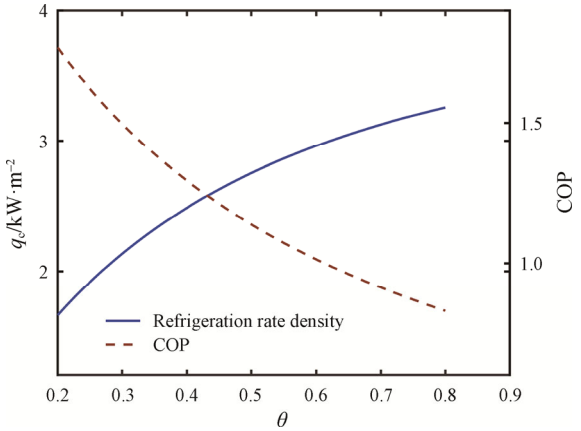

Fig. 9 Refrigeration rate density and the COP versus filling factor

5.1.3 The influence of area thermal resistance

The heat sink and water-cooled plate are used in two sides. Therefore, area thermal resistance of two sides to refrigeration performance should be analyzed, respectively. In this paper, the range of area thermal resistance is selected according to the calculation.

Fig. 10 represents the relationship between refrigeration performance and area thermal resistance when the cold air in the cold side is dissipated through the heat sink. It is clear that when area thermal resistance is constant, the refrigeration rate density increases as the input current density raises, while the COP decreases. When the area thermal resistance is 20×10^{-4} ($m^2\cdot K$)/W, the refrigeration rate density at the input current density j=1.2 A/mm^2 is 1.57 kW/m^2, which is higher than that of at j=0.8 A/mm^2. Furthermore, compared with the COP at j=1.2 A/mm^2, the COP at j=0.8 A/mm^2 increases by 37.33%. With the increase of area thermal resistance, a significant reduction in the refrigeration performance can be observed. When the area thermal resistance of the cold junction is less than 60×10^{-4} ($m^2\cdot K$)/W, the reduction of the area thermal resistance has an obvious influence on the refrigeration rate density and COP.

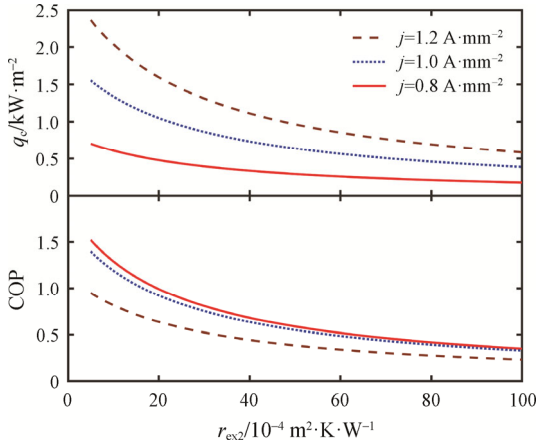

Fig. 10 Refrigeration rate density and the COP versus area thermal resistance of the cold junction

Fig. 11 represents the relationship between refrigeration rate density, COP and area thermal resistance when cooling water in the hot side flows through the water-cooled plate to absorb heat. It should be noted from the figure that the refrigeration performance parameters decrease with the increase of area thermal resistance for fixed input current density. In the case of area thermal resistance from 5×10^{-4} ($m^2\cdot K$)/W to 15×10^{-4} ($m^2\cdot K$)/W, the reduction of refrigeration rate density is 0.33 kW/m^2 at the input current density j=0.8 A/mm^2. However, the reduction is 0.93 kW/m^2 at j=1.2 A/mm^2. Therefore, the smaller the input current density, the smaller the declining rate of the refrigeration rate density. The refrigeration rate density curve drops gently at j=0.8 A/mm^2. Furthermore, when the area thermal resistance of hot junction is 5×10^{-4} ($m^2\cdot K$)/W and the input current density j is 1.2 A/mm^2, 1.0 A/mm^2 and 0.8 A/mm^2, the refrigeration rate density is 2.35 kW/m^2, 1.56 kW/m^2 and 0.78 kW/m^2, respectively. And the COP is 0.89, 1.35 and 1.47, respectively.

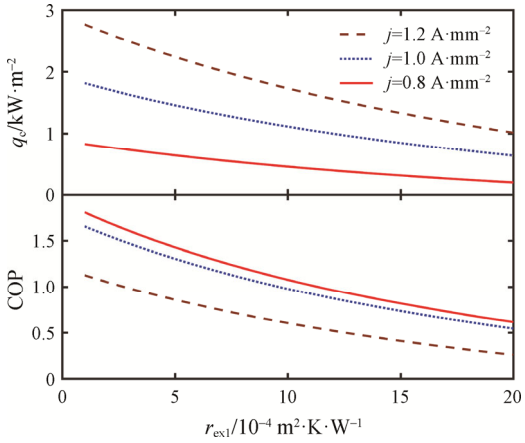

Fig. 11 Refrigeration rate density and the COP versus area thermal resistance of the hot junction

5.2 Heat transfer conditions

5.2.1 The influence of air flow velocity

The structure of heat sink used in the water-cooled thermoelectric air-conditioner is reasonable. Therefore, the geometry of the heat sink and the air flow velocity in the cooling space are studied. The direction of the air flow remains the axial direction. Figs. 12 and 13 show how the refrigeration performance varies as a function of air velocity, rib thickness and rib height, respectively. It should be noted from the figures that the refrigeration performance parameters increase with the decrease of rib thickness for fixed air flow velocity. For instance, when the air flow velocity is 4 m/s, j is 1.0 A/mm^2; fin rib thickness δ_r is 1.5 mm, 2.0 mm and 2.5 mm; the refrigeration rate density is 6.33 kW/m^2, 6.23 kW/m^2 and 6.11 kW/m^2, respectively. The COP is 1.02, 1.00 and 0.98, respectively. Besides, with the increasing value of the air flow velocity, the refrigeration rate density and the COP increase. The increasing rate gradually decreases for fixed rib thickness.

The influences of three kinds of rib heights and air velocity on the refrigeration performance are shown in Figs. 14 and 15, respectively. It is clear that when the air velocity is constant, the refrigeration rate density and COP enhance as the rib height increases. When the air flow velocity is 4 m/s, j is 1.0 A/mm^2, the rib height H is 60 mm, 50 mm and 40 mm, the refrigeration rate density is 6.93 kW/m^2, 6.68 kW/m^2 and 6.33 kW/m^2, respectively. The COP is 1.12, 1.08 and 1.02, respectively. For a given

rib height, as the air velocity increases from 1 m/s to 10 m/s, the refrigeration performance parameters increase, and the increasing rate gradually decreases. When the air velocity is higher than 6 m/s, the influence of enhancement is not obvious. Thus, the air velocity of 6 m/s is suitable for the thermoelectric air-conditioner.

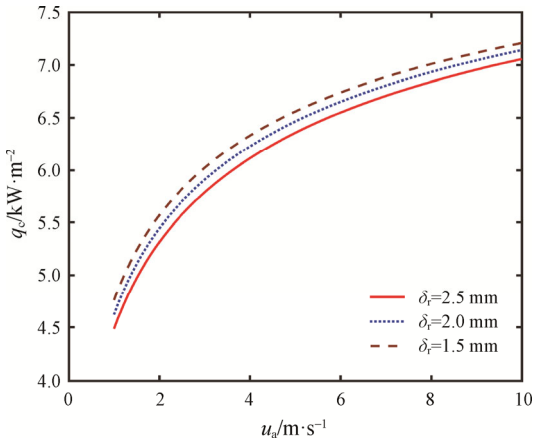

Fig. 12 Refrigeration rate density versus air velocity and fin thickness

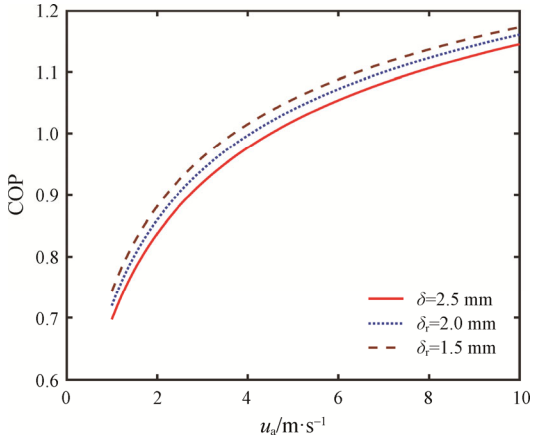

Fig. 13 The COP versus air velocity and fin thickness

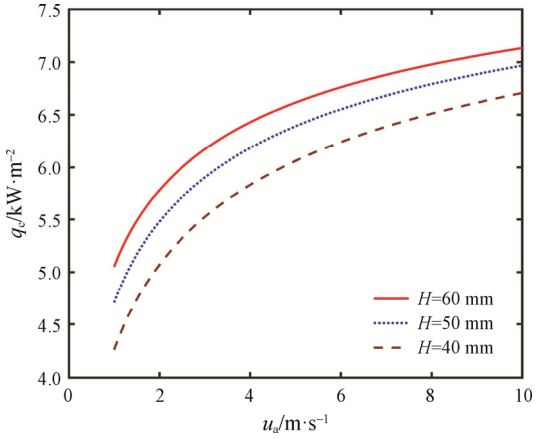

Fig. 14 Refrigeration rate density versus air velocity and fin height

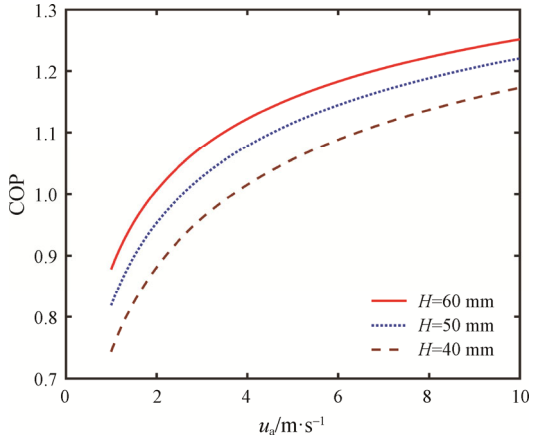

Fig. 15 The COP versus air velocity and fin height

The effects of air velocity, rib thickness and rib height on the area thermal resistance of the cold side are also analyzed. With the increase of the air velocity, the area thermal resistance gradually decreases. When air flow velocity is 6 m/s, area thermal resistances of different rib thicknesses and heights are listed in Table 3. Compared with the rib thickness δ_r=1.5 mm, the area thermal resistance of δ_r=2.0 mm and 2.5 mm increases by 3.95% and 8.69%, respectively. Besides, compared with rib height H=60 mm, the area thermal resistance of H=50 mm and 40 mm increases by 10.59% and 27.60%, respectively. That is, when air velocity is constant, the thinner rib thickness δ_r and higher rib height H lead to a smaller thermal resistance.

Table 3 The area thermal resistances of different rib thicknesses and heights

δ_r/mm	r_{cv2}/10^{-4} m^2·K·W^{-1}	H/mm	r_{cv2}/10^{-4} m^2·K·W^{-1}
1.5	20.25	60	15.87
2.0	21.05	50	17.55
2.5	22.01	40	20.25

5.2.2 The influence of cooling water flow velocity

The velocity and flow direction of water affect the heat absorption of water. The geometry of the water-cooled plate and the cooling water flow velocity in the water-cooled plate are studied. The direction of the water flow remains constant. Figs. 16 and 17 represent the relationship between refrigeration rate density, COP and cooling water flow velocity for three different pipe diameters (d=8 mm, 12 mm, 16 mm). The figures show that as the pipe diameter decreases and flow velocity increases, the refrigeration rate density and the COP increase. When the cooling water flow velocity is 3 m/s, j is 1.0 A/mm^2 and the pipe diameter is 16 mm, 12 mm and 8 mm; the refrigeration rate density is 6.86 kW/m^2, 6.87 kW/m^2 and 6.88 kW/m^2, respectively. And the COP is

approximately the same at 1.11. For a given pipe diameter, the refrigeration rate density and COP increase rapidly when the flow velocity is less than 3 m/s. Therefore, 3 m/s is the optimal flow velocity in the water-cooled thermoelectric air-conditioner according to the design cost.

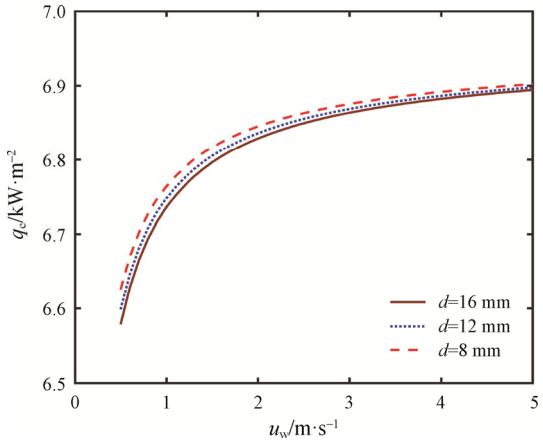

Fig. 16 Refrigeration rate density versus water velocity and pipe diameter

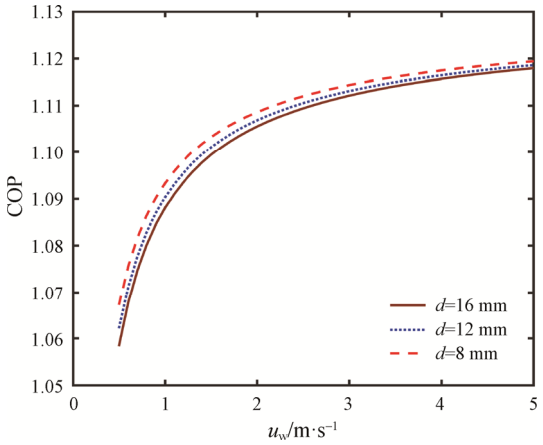

Fig. 17 The COP versus water velocity and pipe diameter

6. Experimental Study

To validate the numerical results, an experimental test set-up is built.

6.1 Experimental test set-up

The experimental test set-up has been completed to verify the model and calculation method. Fig. 18 shows the experimental test set-up. Fig. 19 shows the composition of the experimental system. In the experimental system, cooling water is used in the hot side and the air is used in the cold side, which is to verify the numerical model. The cooling water is pumped from the water tank into the water-cooled plate, and the flow velocity is changed by the water pump. The cooling water absorbs heat through the water-cooled plate in the hot junction, and then flows back to the water tank, which realizes the circulation of cooling water. The cold air in the cooling space releases heat through the heat sink in the cold junction. Because the cooling space is small, the velocity of cold air is changed by the fan and measured by the hot-wire anemometer with accuracy of ±0.03 m/s. If it is necessary to measure air temperature, humidity and carbon dioxide in the laboratory, the ASHRAE standard should be used. The MP3005D DC power is used to supply voltage and input current for the thermoelectric air-conditioner. The voltage stability of DC power is less than 0.05%+1 mV, and the input current stability is less than 0.1%+10 mA. The accuracy of DC power is within ±1.0%. The JK-9000 paperless recorder is used to record data of the temperatures of cooling water and cold air in the cooling space. There are 16 sensing contacts measuring data at the same time. The measuring accuracy of the JK-9000 paperless recorder is within ±0.2% F·S. K-type thermocouple with accuracy of ±0.5 K is used as the sensing contact.

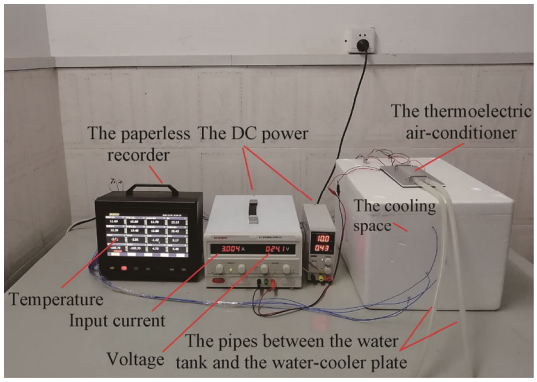

Fig. 18 The experimental test set-up

Fig. 20 shows the water-cooled thermoelectric air-conditioner prototype. The water-cooled thermoelectric air-conditioner contains three TEC-12705 thermoelectric modules. Heat sink and two axial flow fans are used in the cold junction as heat exchanger. The length and width of the rib are 27 mm and 1.5 mm. The heat exchanger in the hot junction is a water-cooled plate with a pipe diameter of 7.5 mm.

Six temperature sensing contacts of the JK-9000 paperless recorder are used to record the temperatures of the air in cooling space and the water in water tank, respectively. As same as the locations of sensing contacts in water tank, one temperature sensing contact is located in the middle of the cooling space, and the rests are distributed in the front and back of the cooling space. The average temperatures of the tested environment and cooling water are obtained, which provide data for

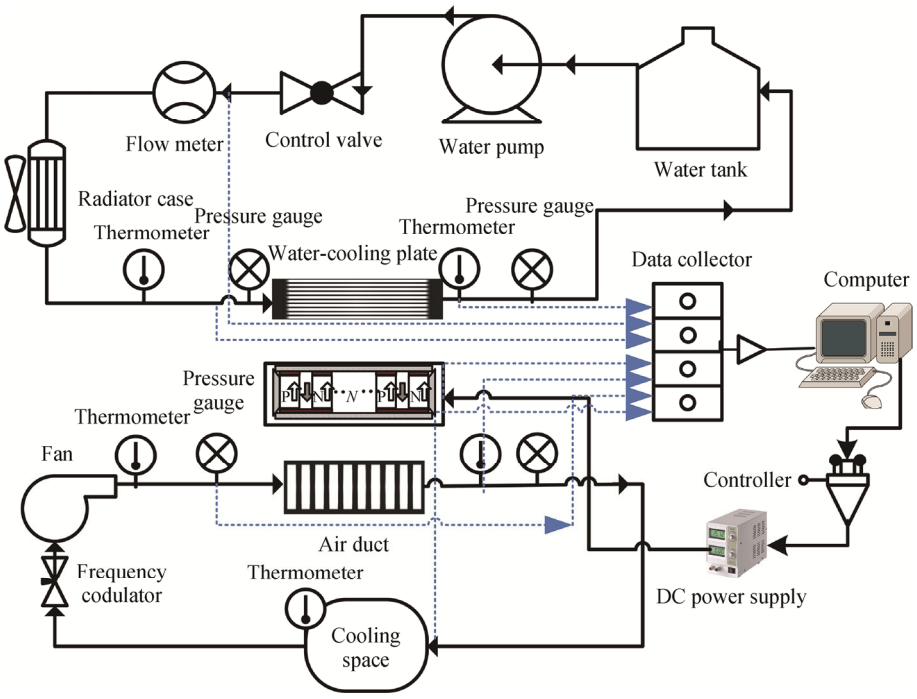

Fig. 19 The experimental test system schematic diagram

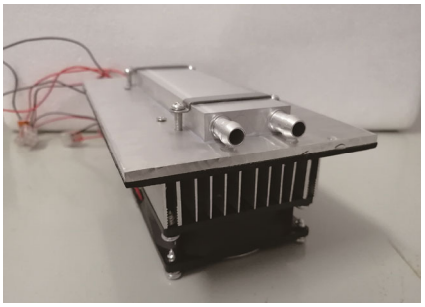

Fig. 20 Thermoelectric air-conditioner of experimental prototype

calculating the refrigeration rate and COP. In addition, the refrigeration rate density can be calculated by the area of thermoelectric modules and refrigeration rate.

The incubator is a 410 mm×290 mm×230 mm foam box with a volume of 27.3 L. In the experiment, the cooling water velocity is 2 m/s, and the air velocity of the axial fan in cooling space is 3 m/s. The test time for a group of experiments is 360 s. The experimental platform has been tested for many times before the experiments. The heat dissipating capacity and the cooling capacity is calculated by the initial and end temperature of cooling water and cold air in the cooling space, respectively. The deviation of energy balance is the comparison between heat dissipating capacity and the sum of cooling capacity and input power. If the deviation of energy balance is large, it indicates that there is a deviation of heat dissipating capacity.

6.2 Experimental validation

Fig. 21 shows the temperature trends of cooling water and cold air versus current in experiment and simulation. In Fig. 21, the solid line represents the simulation with the Thomson effect, and the chain-dotted line represents the simulation without the Thomson effect. The data point is the measurement point, and the dotted line is fitted according to the measurement points. The simulation results show that the temperatures of cooling water and cold air considering the Thomson effect are lower than those without Thomson effect, which indicate that the Thomson effect can improve the refrigeration performance. The deviation is small, especially when the input current is small. However, the deviation increases gradually. As mentioned by Liu et al. [61], Elarusi et al. [62] and He et al. [63], there are three reasons for deviations. First, the temperature of thermoelectric materials rises as the input current increases. The actual resistivity is larger than the theoretical resistivity calculated by average temperature. So, the actual Joule heat is larger than the simulated value. In the experiment, the Joule heat increases with increased input current, which affects the cooling capacity clearly. Second, the water temperature in water tank increases, and the cold air temperature in cooling space decreases as the input current increases. Therefore, the heat transferred between cooling water, cold air and the ambient increases, which causes deviations. Third, the flow resistance of cooling water in the water-cooled plate and air in the heat sink also causes deviations between the experiment and

simulation. In addition, the error of temperature measurement is small. The temperature difference is used to calculate the refrigeration rate and COP in the calculation, so the error of temperature will cancel out and not affect the experimental deviation obviously.

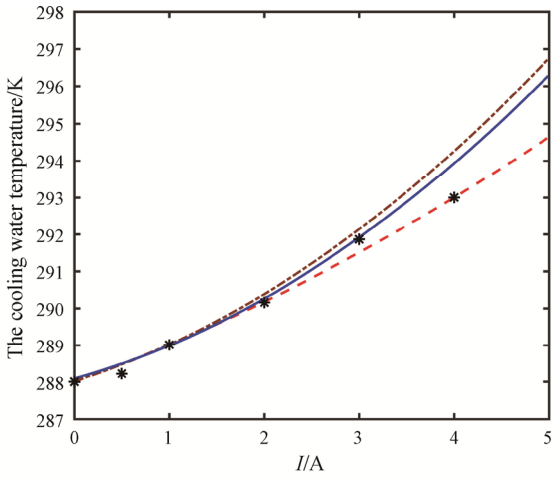

(a) Cooling water temperature

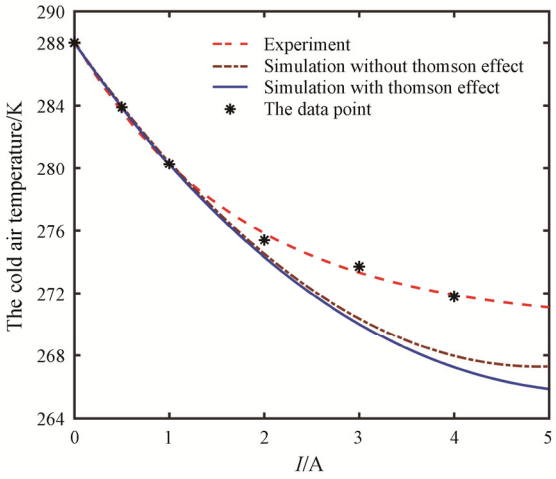

(b) Cold air temperature

Fig. 21 Comparison between temperature trends in experiment and simulation versus current for (a) cooling water temperature and (b) cold air temperature

Table 4 lists the comparison between the refrigeration rate, COP in experiment and simulation when the initial temperatures of ambient, the cooling space and the cooling water are 288 K. In Table 4, $Q_{c,sim}^{\mu>0}$ and $COP_{sim}^{\mu>0}$ are the refrigeration rate and COP when considering Thomson effect; $Q_{c,sim}^{\mu=0}$ and $COP_{sim}^{\mu=0}$ are the refrigeration rate and COP when neglecting Thomson effect. The simulated values of refrigeration rate and COP with Thomson effect are higher than that of without Thomson effect. In addition, when the input current is 0.5 A, the deviation between the experimental and simulated refrigeration rate and COP is 4.1% and 7.5%, respectively. However, when the input current rises to 4.0 A, the deviation between the experimental and simulated refrigeration rate and COP rises to 23.42% and 28.38%, respectively. The deviation of energy balance increases gradually with the increase of input current, so most of the experimental deviation is caused by the inadequate thermal insulation.

Table 4 The refrigeration rate, COP and the deviation in experiment and simulation

I/A	0.5	1.0	2.0	3.0	4.0
$Q_{c,exp}$/W	1.709	3.212	5.253	5.962	6.754
$Q_{c,sim}^{\mu=0}$/W	1.730	3.336	5.864	7.357	8.515
$Q_{c,sim}^{\mu>0}$/W	1.782	3.469	5.969	7.482	8.820
Deviation	4.10%	7.41%	11.99%	20.32%	23.42%
COP_{exp}	0.950	0.417	0.170	0.083	0.053
$COP_{sim}^{\mu=0}$	0.997	0.445	0.198	0.108	0.071
$COP_{sim}^{\mu>0}$	1.027	0.462	0.202	0.110	0.074
Deviation	7.50%	9.74%	15.84%	24.55%	28.38%
Energy balance deviation	6.32%	10.18%	21.52%	30.39%	36.18%

In order to reduce the deviation between experiment and simulation, two measures can be taken. First, a more accurate calculation method of physical parameters of thermoelectric module can be used to reduce the deviation caused by physical parameters in theory. Second, the deviation of energy balance can be reduced by enhancing thermal insulation in the experiment.

7. Conclusions and Future Work

A new analysis method, namely current and refrigeration analysis, is proposed and applied to study the refrigeration performance of water-cooled thermoelectric air-conditioner. An experimental test device is established to verify the theoretical model. Multiple groups of experimental data are obtained. The main results are as follows:

(1) In the water-cooled thermoelectric air-conditioner, the corresponding input current density at the maximum refrigeration rate density is 6.04 A/mm^2, and the corresponding input current density at the maximum COP is 0.62 A/mm^2 at the cooling temperature difference ΔT=5 K. Considering the cooling effect, economy and safety of the water-cooled thermoelectric air-conditioner, the best input current density range should be 0.62 A/mm^2 to 6.04 A/mm^2.

(2) Compared with the cooling temperature difference ΔT=5 K, the maximum refrigeration rate density of ΔT=10 K and 15 K decreases by 13.99% and 27.98%, respectively. And the maximum COP decreases by 57.27% and 76.65%, respectively.

(3) Increasing the filling factor of the thermoelectric module will raise the refrigeration rate density, but the COP will decrease. The COP is an important technical and economic indicator of the refrigeration device. Therefore, it is necessary to select an appropriate filling factor according to the specific design requirements of refrigeration device.

(4) When the air flow velocity is less than 6 m/s or the water flow velocity is less than 3 m/s, the area thermal resistance reduces obviously as the flow velocity raises, and therefore the refrigeration performance is greatly improved.

(5) The deviations are leaded by the physical properties of thermoelectric material and incomplete thermal insulation measures of the device. When the input current increases from 0.5 A to 4.0 A, the deviation of refrigeration rate rises from 4.1% to 23.42%, and the deviation of COP changes from 7.5% to 28.38%.

The future work is to further optimize the area allocation of heat exchangers on both sides to obtain better performance of thermoelectric refrigeration devices for a fixed total area of heat exchangers. Besides, the effect of the properties of different thermoelectric materials on refrigeration performance and the uncertainty propagation analysis will also be studied.

Acknowledgments

This paper is supported by The National Natural Science Foundation of P. R. China (Project No. 11974429 and Project No. 51576207) and the Natural Science Foundation of Naval University of Engineering (20161505).

References

[1] Honig J.M., Harman T.C., Thermoelectric and thermomagnetic effects and applications, McGraw-Hill, New York, 1967.

[2] Riffat S.B., Ma X.L., Thermoelectrics: a review of present and potential applications. Applied Thermal Engineering, 2003, 23(8): 913–935.

[3] Chen L.G., Meng F.K., Sun F.R., Thermodynamic analyses and optimization for thermoelectric devices: The state of the arts. Science China: Technological Sciences, 2016, 59(3): 442–455.

[4] Pourkiaei S.M., Ahmadi M.H., Sadeghzadeh M., Moosavi S., Pourfayaz F., Chen L.G., Pour-Yazdi M.A., Kumar R., Thermoelectric cooler and thermoelectric generator devices: A review of present and potential applications, modeling and materials. Energy, 2019, 186: 115849.

[5] Zhao D.L., Tan G., A review of thermoelectric cooling: Materials, modeling and applications. Applied Thermal Engineering, 2014, 66(1): 15–24.

[6] Liang K., Li Z.H., Chen M., Jiang H.Y., Comparisons between heat pipe, thermoelectric system, and vapour compression refrigeration system for electronics cooling. Applied Thermal Engineering, 2019, 146: 260–267.

[7] Liu D., Zhao F.Y., Yang H.X., Tang G.F., Thermoelectric mini cooler coupled with micro thermosiphon for CPU cooling system. Energy, 2015, 83: 29–36.

[8] Martinez A., Astrain D., Rodriguez A., Aranguren P., Advanced computational model for Peltier effect based refrigerators. Applied Thermal Engineering, 2016, 95: 339–347.

[9] Pourhedayat S., Application of thermoelectric as an instant running-water cooler; experimental study under different operating conditions. Applied Energy, 2018, 229: 364–374.

[10] Saber H.H., AlShehri S.A., Maref W., Performance optimization of cascaded and non-cascaded thermoelectric devices for cooling computer chips. Energy Conversion and Management, 2019, 191: 174–192.

[11] Pietrzyk K., Ohara B., Watson T., Gee M., Avalos D., Lee H., Thermoelectric module design strategy for solid-state refrigeration. Energy, 2016, 114: 823–832.

[12] Sun D.F., Shen L.M., Sun M., Yao Y., Chen H.X., Jin S.P., An effective method of evaluating the device-level thermophysical properties and performance of micro-thermoelectric coolers. Applied Energy, 2018, 219: 93–104.

[13] Gong T.R., Wu Y.J., Gao L., Zhang L., Li J.T., Ming T.Z., Thermo-mechanical analysis on a compact thermoelectric cooler. Energy, 2019, 172: 1211–1224.

[14] Miao Z., Meng X.M., Zhou S., Zhu M.Y., Thermo-mechanical analysis on thermoelectric legs arrangement of thermoelectric modules. Renewable Energy, 2020, 147: 2272–2278.

[15] Wang X.D., Wang Q.H., Xu J.L., Performance analysis of two-stage TECs (thermoelectric coolers) using a three-dimensional heat-electricity coupled model. Energy, 2014, 65: 419–429.

[16] Ma M., Yu J.L., An analysis on a two-stage cascade thermoelectric cooler for electronics cooling applications. International Journal of Refrigeration, 2014, 38: 352–357.

[17] Lin S.M., Yu J.L., Optimization of a trapezoid-type two-stage Peltier couples for thermoelectric cooling applications. International Journal of Refrigeration, 2016, 65: 103–110.

[18] Meng J.H., Wu H.C., Wang T.H., Optimization of two-stage combined thermoelectric devices by a three-dimensional multi-physics model and multi-objective genetic algorithm. Energies, 2019, 12(14):

2832.

[19] Provensi A., Barbosa J.R., Analysis and optimization of air coolers using multiple-stage thermoelectric modules arranged in counter-current flow. International Journal of Refrigeration, 2020, 110: 19–27.

[20] Lv H., Wang T.H., Wang X.D., Meng J.H., Optimal pulse current shape for transient supercooling of thermoelectric cooler. Energy, 2015, 83: 788–796.

[21] Lin S.M., Ma M., Wang J., Yu J.L., Experiment investigation of a two-stage thermoelectric cooler under current pulse operation. Applied Energy, 2016, 180: 628–636.

[22] Ruiz-Ortega P., Olivares-Robles M., Peltier supercooling in transient thermoelectrics: spatial temperature profile and characteristic cooling length. Entropy, 2019, 21(3): 226.

[23] Fong E., Lam T.T., Fischer W.D., Yuan S.W.K., Analytical approach for study of transient performance of thermoelectric coolers. Journal of Thermophysics and Heat Transfer, 2019, 33(1): 96–105.

[24] Baldry M., Timchenko V., Menictas C., Optimal design of a natural convection heat sink for small thermoelectric cooling modules. Applied Thermal Engineering, 2019, 160: 114062.

[25] He Y.J., Cao C., Wu J., Chen G.M., Investigations on coupling between performance and external operational conditons for a simiconductor refrigeration system. International Journal of Refrigeration, 2020, 109: 172–179.

[26] Moradikazerouni A., Afrand M., Alsarraf J., Wongwises S., Asadi A., Nguyen T.K., Investigation of a computer CPU heat sink under laminar forced convection using a structural stability method. International Journal of Heat and Mass Transfer, 2019, 134: 1218–1226.

[27] Moradikazerouni A., Afrand M., Alsarraf J., Mahian O., Wongwises S., Tran M., Comparison of the effect of five different entrance channel shapes of a micro-channel heat sink in forced convection with application to cooling a supercomputer circuit board. Applied Thermal Engineering, 2019, 150: 1078–1089.

[28] Dizaji H.S., Jafarmadar S., Khalilarya S., Moosavi A., An exhaustive experimental study of a novel air-water based thermoelectric cooling unit. Applied Energy, 2016, 181: 357–366.

[29] Gökçek M., Şahin F., Experimental performance investigation of minichannel water cooled-thermoelectric refrigerator. Case Studies in Thermal Engineering, 2017, 10(C): 54–62.

[30] Karwa N., Stanley C., Intwala H., Rosengarten G., Development of a low thermal resistance water jet cooled heat sink for thermoelectric refrigerators. Applied Thermal Engineering, 2017, 111: 1596–1602.

[31] Lin X.H., Mo S.P., Jia L.S., Yang Z., Chen Y., Cheng Z.D., Experimental study and Taguchi analysis on LED cooling by thermoelectric cooler integrated with microchannel heat sink. Applied Energy, 2019, 242: 232–238.

[32] Vo D.D., Alsarraf J., Moradikazerouni A., Afrand M., Salehipour H., Qi C., Numerical investigation of γ-AlOOH nano-fluid convection performance in a wavy channel considering various shapes of nanoadditives. Powder Technology, 2019, 345: 649–657.

[33] Tian Z., Rostami S., Taherialekouhi R., Karimipour A., Moradikazerouni A., Yarmand H., Zulkifli N.W.B.M., Prediction of rheological behavior of a new hybrid nanofluid consists of copper oxide and multi wall carbon nanotubes suspended in a mixture of water and ethylene glycol using curve-fitting on experimental data. Physica A: Statistical Mechanics and its Applications, 2020, 549: 124101.

[34] Alsarraf J., Moradikazerouni A., Shahsavar A., Afrand M., Salehipour H., Tran M.D., Hydrothermal analysis of turbulent boehmite alumina nanofluid flow with different nanoparticle shapes in a minichannel heat exchanger using two-phase mixture model. Physica A: Statistical Mechanics and its Applications, 2019, 520: 275–288.

[35] Ma Y.L., Shahsavar A., Moradi I., Rostami S., Moradikazerouni A., Yarmand H., Zulkifli N.W.B.M., Using finite volume method for simulating the natural convective heat transfer of nano-fluid flow inside an inclined enclosure with conductive walls in the presence of a constant temperature heat source. Physica A: Statistical Mechanics and its Applications, 2019: 123035.

[36] Ahammed N., Asirvatham L.G., Wongwises S., Entropy generation analysis of graphene-alumina hybrid nanofluid in multiport minichannel heat exchanger coupled with thermoelectric cooler. International Journal of Heat and Mass Transfer, 2016, 103: 1084–1097.

[37] Sun X.Q., Ling L., Liao S.G., Chu Y.H., Fan S.Y., Mo Y.J., A thermoelectric cooler coupled with a gravity-assisted heat pipe: An analysis from heat pipe perspective. Energy Conversion and Management, 2018, 155: 230–242.

[38] Liu Y., Su Y., Experimental investigations on COPs of thermoelectric module frosting systems with various hot side cooling methods. Applied Thermal Engineering, 2018, 144: 747–756.

[39] Tan G., Zhao D.L., Study of a thermoelectric space cooling system integrated with phase change material. Applied Thermal Engineering, 2015, 86: 187–198.

[40] Jiang L., Zhang H.Y., Li J.W., Xia P., Thermal performance of a cylindrical battery module impregnated with PCM composite based on thermoelectric cooling. Energy, 2019: 116048.

[41] Andresen B., Berry R.S., Ondrechen M.J., Salamon P., Thermodynamics for processes in finite time. Accounts of Chemical Research, 1984, 17(8): 266–271.

[42] Chen L.G., Wu C., Sun F.R., Finite time thermodynamic optimization or entropy generation minimization of energy systems. Journal of Non-Equilibrium Thermodynamics, 1999, 24(4): 327–359.

[43] Chen L.G., Xia S.J., Progresses in generalized thermodynamic dynamic-optimization of irreversible processes. Scientia Sinica: Technologica, 2019, 49(9): 981–1022.

[44] Chen L.G., Xia S.J., Feng H.J., Progress in generalized thermodynamic dynamic-optimization of irreversible cycles. Scientia Sinica: Technologica, 2019, 49(11): 1223–1267. (in Chinese)

[45] Chen L.G., Li J., Thermodynamic optimization theory for two-heat-reservoir cycles, Science Press, Beijing, 2020 (in Chinese).

[46] Chen L.G., Gong J.Z., Shen L.W., Sun F.R., Wu C., Theoretical analysis and experimental confirmation for the performance of thermoelectric refrigerator. Journal of Non-Equilibrium Thermodynamics, 2001, 26(1): 85–92.

[47] Meng F.K., Chen L.G., Sun F.R., Performance prediction and irreversibility analysis of a thermoelectric refrigerator with finned heat exchanger. Acta Physica Polonica A, 2011, 120(3): 397–406.

[48] Chen L.G., Meng F.K., Xie Z.H., Ding Z.M., Xia S.J., Feng H.J., Thermodynamic modeling and analysis of an air-cooled small space thermoelectric cooler. The European Physical Journal Plus, 2020, 135(1): 80.

[49] Lu X., Zhao D.L., Ma T., Wang Q.W., Fan J.T., Yang R.G., Thermal resistance matching for thermoelectric cooling systems. Energy Conversion and Management, 2018, 169: 186–193.

[50] Lundgaard C., Sigmund O., Design of segmented thermoelectric Peltier coolers by topology optimization. Applied Energy, 2019, 239: 1003–1013.

[51] Sun H.N., Gil S.U., Liu W., Liu Z.C., Structure optimization and exergy analysis of a two-stage TEC with two different connections. Energy, 2019, 180: 175–191.

[52] Chen W.H., Liao C.Y., Hung C.I., A numerical study on the performance of miniature thermoelectric cooler affected by Thomson effect. Applied Energy, 2012, 89(1): 464–473.

[53] Ruiz-Ortega P., Olivares-Robles M., Analysis of a hybrid thermoelectric microcooler: thomson heat and geometric optimization. Entropy, 2017, 19(7): 312.

[54] Kaushik S.C., Manikandan S., The influence of Thomson effect in the performance optimization of a two-stage thermoelectric cooler. Cryogenics, 2015, 72: 57–64.

[55] Feng Y.L., Chen L.G., Meng F.K., Sun F.R., Thermodynamic analysis of TEG-TEC device including influence of Thomson effect. Journal of Non-Equilibrium Thermodynamics, 2018, 43: 75–86.

[56] Incropera F., Witt D.D., Fundamentals of heat and mass transfer, 6th ed, Wiley, New York, 2007.

[57] Eckert E.R.G., Drake R.M., Analysis of heat and mass transfer, McGraw-Hill, New York, 1972.

[58] Cengel Y.A., Heat transfer: A practical approach, McGraw-Hill, New York, 1998.

[59] Thermoelectric Handbook. http://www.Laridtech.com, 2010.

[60] Meng F.K., Chen L.G., Sun F.R., A numerical model and comparative investigation of a thermoelectric generator with multi-irreversibilities. Energy, 2011, 36(5): 3513–3522.

[61] Liu Z.B., Zhang L., Gong G.C., Luo Y.Q., Meng F.F., Experimental study and performance analysis of a solar thermoelectric air conditioner with hot water supply. Energy and Buildings, 2015, 86: 619–625.

[62] Elarusi A., Attar A., Lee H., Analysis and experimental investigation of optimum design of thermoelectric cooling/heating system for Car Seat Climate Control (CSCC). Journal of Electronic Materials, 2018, 47(2): 1311–1321.

[63] He W., Zhou J.Z., Hou J.X., Chen C., Ji J., Theoretical and experimental investigation on a thermoelectric cooling and heating system driven by solar. Applied Energy, 2013, 107: 89–97.